

CsV₃Sb₅: A \mathbb{Z}_2 Topological Kagome Metal with a Superconducting Ground State

Brenden R. Ortiz,^{1,*} Samuel M. L. Teicher¹, Yong Hu², Julia L. Zuo,¹ Paul M. Sarte,¹ Emily C. Schueller,¹ A. M. Milinda Abeykoon,³ Matthew J. Krogstad⁴, Stephan Rosenkranz⁴, Raymond Osborn⁴, Ram Seshadri,¹ Leon Balents⁵, Junfeng He,² and Stephen D. Wilson^{1,†}

¹Materials Department and California Nanosystems Institute, University of California Santa Barbara, Santa Barbara, California 93106, USA

²Hefei National Laboratory for Physical Sciences at the Microscale, Department of Physics and CAS Key Laboratory of Strongly-coupled Quantum Matter Physics, University of Science and Technology of China, Hefei, Anhui 230026, China

³National Synchrotron Light Source II, Brookhaven National Laboratory, Upton, New York 11973, USA

⁴Materials Science Division, Argonne National Laboratory, Lemont, Illinois 60439-4845, USA

⁵Kavli Institute for Theoretical Physics, University of California, Santa Barbara, Santa Barbara, California 93106, USA



(Received 2 August 2020; accepted 4 November 2020; published 10 December 2020)

Recently discovered alongside its sister compounds KV₃Sb₅ and RbV₃Sb₅, CsV₃Sb₅ crystallizes with an ideal kagome network of vanadium and antimonene layers separated by alkali metal ions. This work presents the electronic properties of CsV₃Sb₅, demonstrating bulk superconductivity in single crystals with a $T_c = 2.5$ K. The normal state electronic structure is studied via angle-resolved photoemission spectroscopy and density-functional theory, which categorize CsV₃Sb₅ as a \mathbb{Z}_2 topological metal. Multiple protected Dirac crossings are predicted in close proximity to the Fermi level (E_F), and signatures of normal state correlation effects are also suggested by a high-temperature charge density wavelike instability. The implications for the formation of unconventional superconductivity in this material are discussed.

DOI: [10.1103/PhysRevLett.125.247002](https://doi.org/10.1103/PhysRevLett.125.247002)

Kagome metals are a rich frontier for the stabilization of novel correlated and topological electronic states. Depending on the degree of electron filling within the kagome lattice, a wide array of instabilities are possible, ranging from bond density wave order [1,2], charge fractionalization [3,4], spin liquid states [5], charge density waves [6], and superconductivity [1,7]. Additionally, the kagome structural motif imparts the possibility of topologically nontrivial electronic structures, where the coexistence of Dirac cones and flatbands promoting strong correlation effects may engender correlated topological states. For instance, the presence of magnetic order [8–10] in kagome compounds has been noted to stabilize novel quantum anomalous Hall behaviors, and electron-electron interactions in certain scenarios are proposed to drive the formation of topological insulating phases [11].

One widely sought electronic instability on a two-dimensional kagome lattice is the formation of a superconducting ground state. Layered kagome metals that superconduct are rare, and the interplay between the nontrivial topology accessible via their electronic band structures and the formation of an intrinsic superconducting state makes this a particularly appealing space for realizing exotic ground states and quasiparticles. Unconventional superconductivity is predicted to emerge via nesting-driven interactions in heavily doped kagome lattices [12]. This mechanism, first pointed out in theories for doped graphene (which shares the

hexagonal symmetry of the kagome lattice) [13,14], relies upon scattering between saddle points of a band at the M points of the 2D Brillouin zone, which are relevant when the system possesses a nearly hexagonal Fermi surface proximate to a topological transition. Superconductivity potentially competes with a variety of other electronic instabilities at different fillings [11,15]. Realizing superconductivity in a two-dimensional kagome material that avoids these competing instabilities remains an open challenge.

Recently, a new family of layered kagome metals that crystallize in the AV₃Sb₅ structure ($A = \text{K, Rb, Cs}$) was reported [16]. These materials crystallize into the $P6/mmm$ space group, with a kagome network of vanadium cations coordinated by octahedra of Sb. The compounds are layered, with the kagome sheets separated by layers of the A-site alkali metal ions (Fig. 1). Compounds across the series are high-mobility, two-dimensional metals with signatures of correlation effects and potential electronically driven symmetry breaking. Recent studies have further shown that one variant, KV₃Sb₅, is a Dirac semimetal with an extraordinarily large anomalous Hall effect in the absence of long-range magnetic order [17]. Remarkably little, however, remains known about this new class of kagome metals, particularly with regards to their capacity for hosting correlated topological states.

Here we identify that CsV₃Sb₅, the heaviest member of the new kagome compounds, is a \mathbb{Z}_2 topological metal with

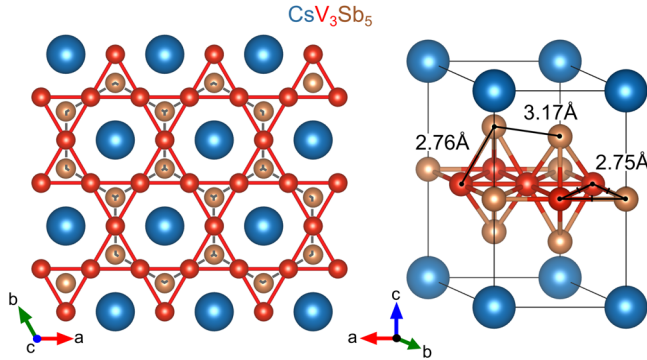


FIG. 1. CsV_3Sb_5 is a layered compound with a structurally perfect kagome network of vanadium. There are two distinct Sb sites in the structure: (1) a simple hexagonal net woven into the kagome layer and (2) graphitelike layers of antimony (antimonene) above and below the kagome layer. All bonds ≤ 3.2 Å have been drawn in the isometric perspective.

a superconducting ground state. Angle-resolved photoemission spectroscopy (ARPES) measurements combined with density-functional theory (DFT) calculations reveal the presence of multiple Dirac points near the Fermi level and predict topologically protected surface states only 0.05 eV above the Fermi level at the M points. Furthermore, both ARPES and DFT observe hexagonal Fermi surfaces, consistent with close proximity of saddle points at M . Magnetization, heat capacity, and electrical resistivity measurements reveal the onset of superconductivity at $T_c = 2.5$ K and further identify a higher-temperature $T^* = 94$ K transition suggestive of charge density wave order. Our work establishes CsV_3Sb_5 as a novel exfoliable, kagome metal with a superconducting ground state and protected Dirac crossings close to E_F .

Single crystals of CsV_3Sb_5 were synthesized via a self-flux growth method [18]. Magnetization measurements were performed using a Quantum Design superconducting quantum interference device magnetometer (MPMS3) in vibrating-sample measurement mode, and resistivity and heat capacity measurements were performed using a Quantum Design Dynacool physical properties measurement system. ARPES measurements were obtained at the Stanford Synchrotron Radiation Lightsource (SSRL, beam line 5-2), a division of the SLAC National Accelerator Laboratory, using 120 eV photons with an energy resolution better than 20 meV. Temperature-dependent x-ray diffraction data were collected at Brookhaven National Laboratory (beam line 28-ID-1) and at the Advanced Photon Source at Argonne National Laboratory (sector 6-ID-D). Rietveld refinements of temperature-dependent diffraction were performed using TOPAS Academic V6 [34]. Structure visualization was performed with the VESTA software package [19], and the electronic structure of CsV_3Sb_5 was calculated in VASP v5.4.4 [35–37] using projector-augmented wave potentials [38,39] with details described in Supplemental Material [18].

For an intuitive understanding of the CsV_3Sb_5 structure, we first consider the constituent sublattices. The hallmark two-dimensional kagome network is formed by the V1 sublattice and is interpenetrated by a simple hexagonal net of Sb1 antimony. All interatomic distances within the kagome layer are equal (2.75 Å), as required by the high symmetry of the V1 (Wyckoff $3g$) and Sb1 (Wyckoff $1b$) sites. The Sb2 sublattice creates graphitelike layers of Sb (antimonene) that encapsulate the kagome sheets. The Cs1 sublattice naturally fills the space between the graphitelike sheets, and the nearest Cs-Sb distance is nearly 4 Å.

Bulk electronic properties of CsV_3Sb_5 were studied via electron transport, magnetization, and heat capacity measurements. Figures 2(a)–2(c) show characterization data collected across a broad range of temperatures. Magnetization data collected under $\mu_0 H = 1$ T are plotted as susceptibility $\chi = (M/H)$ in Fig. 2(a) and show a high-temperature response ($T > 100$ K) consistent with Pauli paramagnetism. As a rough estimate, DFT calculations of the density of states at the Fermi level $g(E_F) \approx 10 \text{ eV}^{-1} \text{ cell}^{-1}$ estimate $\chi \approx 200 \times 10^{-6} \text{ emu Oe}^{-1} \text{ mol}^{-1}$, which agrees reasonably well with the experimental data.

At temperatures below 94 K, a sharp drop in the magnetization data denotes the onset of a phase transition, noted as T^* . This transition also appears as an inflection point in the resistivity data shown in Fig. 2(b), where temperature-dependent resistivity data with current flowing both in the kagome planes (ρ_{ab}) and between the planes (ρ_c) are plotted. The out-of-plane resistivity is nearly 600 times larger than in plane, emphasizing the two-dimensional nature of the Fermi surface. Heat capacity data plotted in Fig. 2(c) also illustrate a strong entropy anomaly at $T^* = 94$ K. The integrated entropy released through the T^* transition is approximately $\Delta S = 1.6 \text{ J mol}^{-1} \text{ K}^{-1}$ and is naively too small to account for collective spin freezing of free V moments. Instead, it likely arises from freezing within the charge sector [11], suggesting a potential charge or bond density wave anomaly that will be discussed later in this Letter.

Figures 2(d)–2(f) show the onset of superconductivity in magnetization, resistivity, and heat capacity, respectively. In all cases, the onset of superconductivity occurs at approximately $T_c = 2.5$ K. Magnetization data reveal bulk superconductivity and a well-defined Meissner state, and heat capacity measurements show a sharp entropy anomaly at the superconducting transition, although, due to a limited temperature regime, we are unable to fully characterize the gapped behavior far below T_c . The slight offset in the onset of T_c in electrical resistivity [Fig. 2(e)] measurements is due to the high probe currents (8 mA) used in the dc measurement. Reduced currents show T_c return to nominal values, although the data quality suffers significantly due to the low resistivity of CsV_3Sb_5 single crystals.

Having determined that CsV_3Sb_5 is a bulk kagome superconductor with a transition temperature $T_c = 2.5$ K,

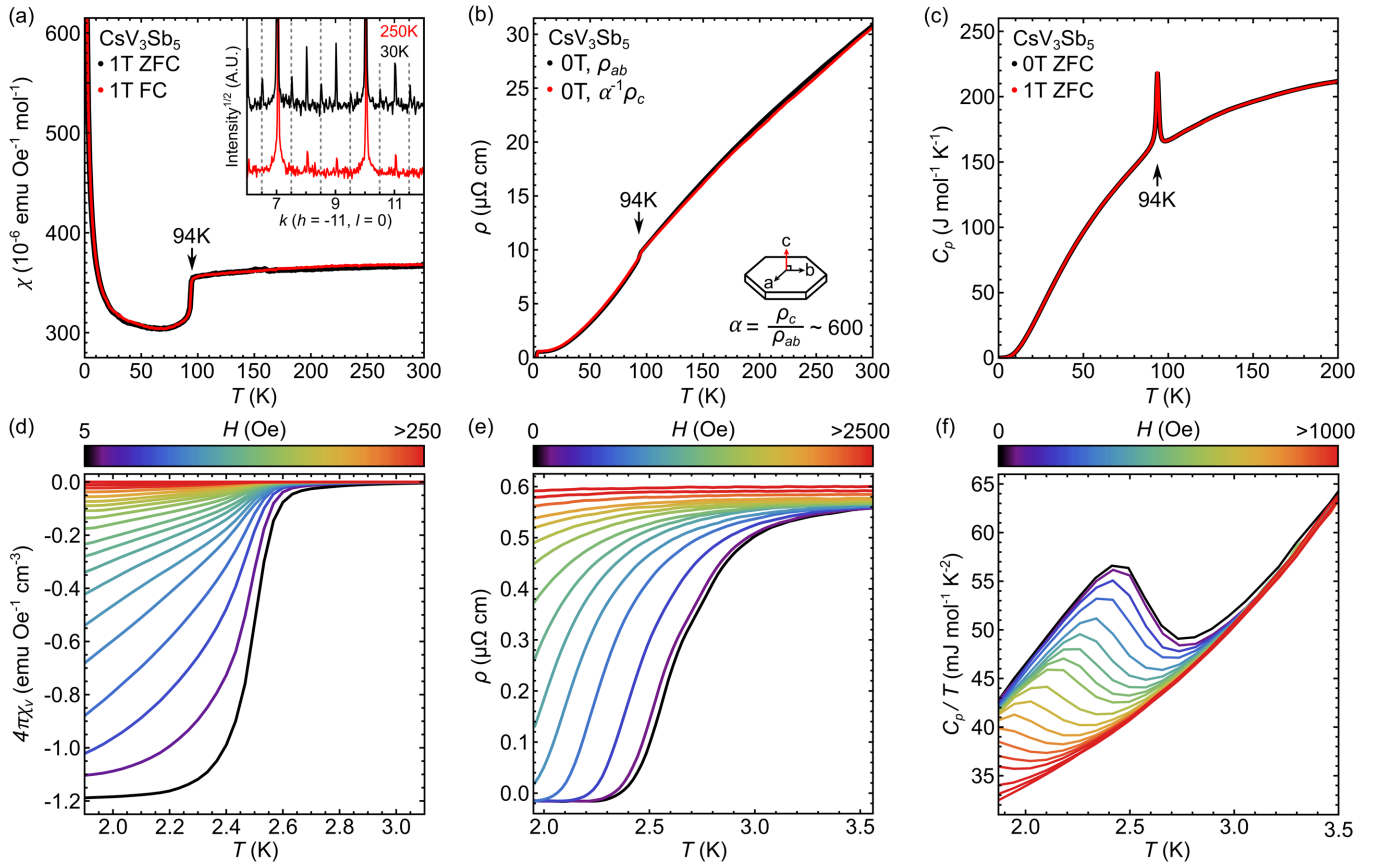


FIG. 2. (a),(c),(e) Full temperature ranges for the magnetization, electrical resistivity, and heat capacity, respectively, shown for single crystals of CsV_3Sb_5 . All measurements indicate the presence of an anomaly T^* at 94 K, suspected to be an electronic instability (e.g., charge ordering). The inset in (a) shows line cuts through x-ray diffraction data below and above T^* . Dashed lines denote the appearance of half-integer reflections. (b),(d),(f) Field-dependent measurements at low temperatures, showing the onset of superconductivity in magnetization, resistivity, and heat capacity, respectively. The T_c for CsV_3Sb_5 is approximately 2.5 K, with a slight suppression in resistivity due to high probe currents.

we next examine the normal state metal via a combination of ARPES measurements and DFT modeling. Figure 3(a) shows both ARPES and DFT modeling data with the hexagonal Brillouin zone superimposed on the $E = 0$ eV constant energy contour and high-symmetry points K , M , and Γ labeled. Data collected with differing photon energies did not reveal any appreciable dispersion along k_z , consistent with a quasi-2D band structure. ARPES data were collected at 50, 80, 100, and 120 K, and no resolvable changes were observed in the band structure when transitioning through the T^* transition. The DFT model shows remarkable agreement with the ARPES data, recovering all experimental observed crossings below the Fermi level. Figure 3(b) shows both the measured and calculated electronic structure hosts multiple Dirac points at finite binding energies.

While inaccessible in the present ARPES data, the DFT model further reveals multiple topological band features slightly above the Fermi energy. The \bar{M} point is of particular interest, as M is a time-reversal invariant momentum (TRIM) point. Figure 4 shows the results of a tight-binding

calculation of surface states in CsV_3Sb_5 , where bright spots slightly above the Fermi energy indicate surface states.

Unlike many heavily studied kagome lattices [e.g., $\text{ZnCu}_3(\text{OH})_6\text{Cl}_2$ [40–42], Fe_3Sn_2 [9,43], Mn_3Ge [44,45], and $\text{Co}_3\text{Sn}_2\text{S}_2$ [10,46,47]], CsV_3Sb_5 does not exhibit resolvable magnetic order. Given that CsV_3Sb_5 possesses both time-reversal and inversion symmetry as well as a continuous, symmetry-enforced, direct gap at every k point, one can calculate the \mathbb{Z}_2 topological invariant between each pair of bands near the Fermi level by simply analyzing the parity of the wave function at the TRIM points [48]. This analysis reveals a number of topologically nontrivial crossings between adjacent bands in the region ± 1 eV from the Fermi level. For clarity, we will focus on the surface states crossing at the \bar{M} point here with further analysis presented in Supplemental Material [18]. Figure 4(b) presents a close-up of the calculated surface states near the \bar{M} point. The surface states at the \bar{M} point manifest approximately 0.05 eV above the Fermi energy. The apparent anisotropy in the calculated surface state dispersions ($\bar{M}-\bar{K}$ versus $\bar{M}-\bar{\Gamma}$) derives from the direct “gap” moving up or down in energy

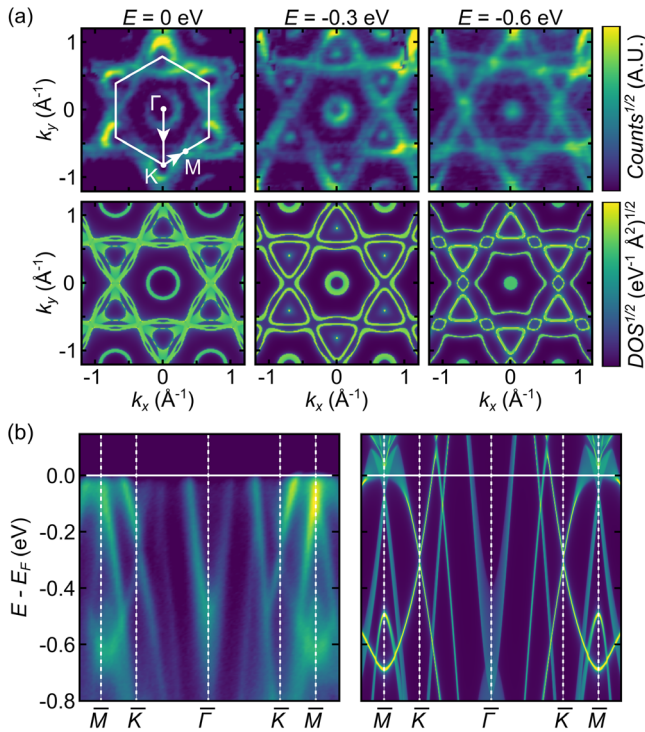


FIG. 3. Experimental ARPES data and comparison with DFT calculations. (a) A selection of constant energy maps at 80 K are compared with DFT calculations, showing excellent agreement. The hexagonal Brillouin zone is superimposed on the $E = 0$ eV data. (b) ARPES and DFT data tracing from M - K - Γ - K - M reveal multiple Dirac points throughout the dispersion. Surface states can be observed in the DFT data at the M point, slightly above E_F .

depending on direction away from the \bar{M} point. This is not uncommon among topological metals [49–51].

Topologically nontrivial surface states close to E_F and the continuous direct gap throughout the Brillouin zone allow the identification of the normal state as a \mathbb{Z}_2 topological metal [52,53]. The T^* transition in this compound also suggests that electronic interactions are appreciable in this material. This transition is accompanied by a subtle change in the derivative of the lattice parameters, cell volume, and associated crystallographic parameters upon crossing T^* [18]. Single-crystal x-ray diffraction further shows the formation of a weak superlattice of charge scattering at half-integer reflections [an example shown in the inset in Fig. 2(a)] [18].

The presence of a weak, structural superlattice is suggestive of a secondary structural response to a primary electronic order parameter such as a charge or bond density wave instability. Theoretical studies of partially filled kagome lattices predict a wide array of electronic order parameters [11]. The metallic nature of CsV_3Sb_5 and its high degree of covalency makes formal charge assignment imprecise; however, in the ionic limit, the kagome lattice of V sites would possess one electron per triangle (1/6

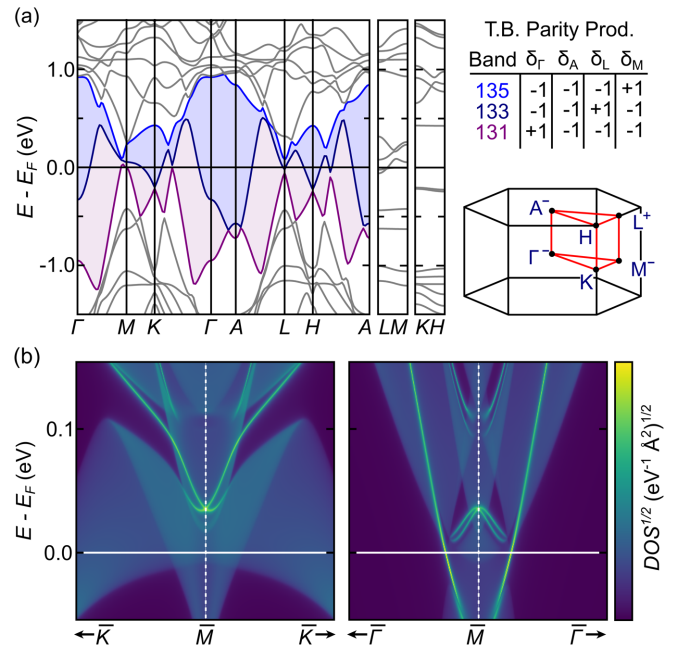


FIG. 4. (a) Calculated band structure of CsV_3Sb_5 along high-symmetry directions across the Brillouin zone. A continuous direct gap (shaded) is noted and high-symmetry points in the BZ are labeled. (b) Tight-binding model of CsV_3Sb_5 showing topologically protected surface states that manifest at the time-reversal invariant momentum \bar{M} point.

filling). Charge density wave (CDW) order with a $(\pi, 0)$ in-plane wave vector consistent with our single-crystal x-ray diffraction data is predicted in spinful models and spinless fermion models of interacting electrons in a partially filled kagome lattice [11].

Nesting across a two-dimensional Fermi surface with an underlying hexagonal motif is also thought to promote the formation of a superconducting state [14]. Competing density wave instabilities may also arise, and, in the present case, scattering along the $(\pi, 0)$ wave vector would connect an enhanced density of states at saddle points near the Fermi energy at the M points in CsV_3Sb_5 's band structure. To our knowledge, this is the first material example hosting the band structure, Fermi energy, and ground state requisite for this theoretical mechanism. Given the CDW-like instability observed at T^* in this compound, interactions along this wave vector are likely enhanced and may promote a competition between CDW and superconducting instabilities. Although a structural superlattice exists, ARPES data do not resolve spectral broadening of the Fermi surface across the nested M points, consistent with the long-range, weak nature of the high-temperature density wave order. Unconventional superconductivity with chiral d -wave pairing may emerge in this scenario [1,13].

Superconductivity manifest within an electronically two-dimensional kagome lattice is rare unto itself. While other materials with kagome networks embedded within their lattice structures are known to superconduct (e.g., in certain

silicides and borides [54,55]), all of these examples are inherently three-dimensional both structurally and electronically. CsV_3Sb_5 seemingly opens a unique opportunity for mapping to models of nesting-driven instabilities emergent within a two-dimensional kagome metal. Isostructural variants KV_3Sb_5 and RbV_3Sb_5 host similar T^* transitions at 80 and 104 K, respectively, likely indicative of a similar high-temperature density wave order [16]; however, superconductivity has been observed only in CsV_3Sb_5 to date. Understanding the interplay between the potentially competing T^* order parameter and the formation of superconductivity across the AV_3Sb_5 family is an interesting topic for future study.

The \mathbb{Z}_2 topological band structure of CsV_3Sb_5 may also be of interest for stabilizing the formation of Majorana modes within the vortex cores of a natively proximitized, superconducting surface state. Materials hosting both topologically nontrivial surface states and a native superconducting ground state are uncommon, with relatively few promising candidates identified in $\text{FeSe}_{(1-x)}\text{Te}_x$ [56–60], doped Bi_2Se_3 [61–65], and $\text{Sn}_{(1-x)}\text{In}_x\text{Te}$ [66–68]. With relatively light electron doping (such as Ba substitution), CsV_3Sb_5 can likely be driven into a regime where such a proximitized topological surface state could be tested.

In summary, our results demonstrate that kagome metals can serve as a rich arena for exploring the interplay between correlated electron effects and superconductivity within a topologically nontrivial band structure. Our results demonstrate bulk superconductivity with $T_c = 2.5$ K in single crystals of CsV_3Sb_5 and classify its normal state as a \mathbb{Z}_2 topological metal with multiple topologically nontrivial band crossings in close proximity to the Fermi level. An anomalous CDW-like transition in the normal state suggests strong correlation effects and an electronic instability that weakly couples to the lattice. Future studies exploring the relation between this instability and the potential emergence of nesting-driven, unconventional superconductivity on the kagome lattice is motivated by our present results.

S. D. W., R. S., L. B., and B. R. O. acknowledge support from the University of California Santa Barbara Quantum Foundry, funded by the National Science Foundation (NSF DMR-1906325). Research reported here also made use of shared facilities of the UC Santa Barbara Materials Research Science and Engineering Center (NSF DMR-1720256). B. R. O. and P. M. S. also acknowledge support from the California NanoSystems Institute through the Elings fellowship program. S. M. L. T. has been supported by the National Science Foundation Graduate Research Fellowship Program under Grant No. DGE-1650114. This research used resources of the Advanced Photon Source, a U.S. Department of Energy (DOE) Office of Science User Facility operated for the DOE Office of Science by Argonne National Laboratory under Contract No. DE-

AC02-06CH11357. J.-F. H. and Y. H. were supported by the USTC start-up fund. The ARPES measurements were carried out under the user proposal program of SSRL, which is operated by the Office of Basic Energy Sciences, U.S. DOE, under Contract No. DE-AC02-76SF00515. This research used beam line 28-ID-1 of the National Synchrotron Light Source II, a U.S. Department of Energy (DOE) Office of Science User Facility operated for the DOE Office of Science by Brookhaven National Laboratory under Contract No. DE-SC0012704. Shared computing facilities of the Center for Scientific Computing at UC Santa Barbara, supported by NSF CNS-1725797. Work at the Materials Science Division at Argonne National Laboratory (single crystal diffuse scattering) was supported by the US Department of Energy, Office of Science, Office of Basic Energy Sciences, Materials Sciences and Engineering Division.

*ortiz.brendenr@gmail.com

†stephendwilson@ucsb.edu

- [1] W.-S. Wang, Z.-Z. Li, Y.-Y. Xiang, and Q.-H. Wang, *Phys. Rev. B* **87**, 115135 (2013).
- [2] S. V. Isakov, S. Wessel, R. G. Melko, K. Sengupta, and Y. B. Kim, *Phys. Rev. Lett.* **97**, 147202 (2006).
- [3] A. O'Brien, F. Pollmann, and P. Fulde, *Phys. Rev. B* **81**, 235115 (2010).
- [4] A. Rüegg and G. A. Fiete, *Phys. Rev. B* **83**, 165118 (2011).
- [5] S. Yan, D. A. Huse, and S. R. White, *Science* **332**, 1173 (2011).
- [6] H.-M. Guo and M. Franz, *Phys. Rev. B* **80**, 113102 (2009).
- [7] W.-H. Ko, P. A. Lee, and X.-G. Wen, *Phys. Rev. B* **79**, 214502 (2009).
- [8] M. Kang, L. Ye, S. Fang, J.-S. You, A. Levitan, M. Han, J. I. Facio, C. Jozwiak, A. Bostwick, E. Rotenberg *et al.*, *Nat. Mater.* **19**, 163 (2020).
- [9] L. Ye, M. Kang, J. Liu, F. Von Cube, C. R. Wicker, T. Suzuki, C. Jozwiak, A. Bostwick, E. Rotenberg, D. C. Bell *et al.*, *Nature (London)* **555**, 638 (2018).
- [10] N. Morali, R. Batabyal, P. K. Nag, E. Liu, Q. Xu, Y. Sun, B. Yan, C. Felser, N. Avraham, and H. Beidenkopf, *Science* **365**, 1286 (2019).
- [11] J. Wen, A. Rüegg, C. C. Joseph Wang, and G. A. Fiete, *Phys. Rev. B* **82**, 075125 (2010).
- [12] S.-L. Yu and J.-X. Li, *Phys. Rev. B* **85**, 144402 (2012).
- [13] R. Nandkishore and A. V. Chubukov, *Phys. Rev. B* **86**, 115426 (2012).
- [14] R. Nandkishore, L. Levitov, and A. Chubukov, *Nat. Phys.* **8**, 158 (2012).
- [15] M. L. Kiesel, C. Platt, and R. Thomale, *Phys. Rev. Lett.* **110**, 126405 (2013).
- [16] B. R. Ortiz, L. C. Gomes, J. R. Morey, M. Winiarski, M. Bordelon, J. S. Mangum, I. W. H. Oswald, J. A. Rodriguez-Rivera, J. R. Neilson, S. D. Wilson *et al.*, *Phys. Rev. Mater.* **3**, 094407 (2019).
- [17] S.-Y. Yang, Y. Wang, B. R. Ortiz, D. Liu, J. Gayles, E. Derunova, R. Gonzalez-Hernandez, L. Smejkal, Y. Chen, S. S. Parkin *et al.*, *Sci. Adv.* **6**, eabb6003 (2020).

- [18] See Supplemental Material at <http://link.aps.org/supplemental/10.1103/PhysRevLett.125.247002> for experimental and theoretical details and supporting results, which includes Refs. [19–33].
- [19] K. Momma and F. Izumi, *J. Appl. Crystallogr.* **44**, 1272 (2011).
- [20] J. Sangster and A. Pelton, *J. Phase Equilib.* **18**, 382 (1997).
- [21] A. Hammersley, S. Svensson, M. Hanfland, A. Fitch, and D. Hausermann, *High Press. Res.* **14**, 235 (1996).
- [22] S. P. Westrip, *J. Appl. Crystallogr.* **43**, 920 (2010).
- [23] G. Jennings, Crystal coordinate transformation workflow (CCTW), software available at <https://sourceforge.net/projects/cctw/>.
- [24] R. Osborn and J. Wozniak, NexPy,” software available at <https://github.com/nexpy/nexpy>.
- [25] J. Sun, A. Ruzsinszky, and J. P. Perdew, *Phys. Rev. Lett.* **115**, 036402 (2015).
- [26] S. Grimme, *J. Comput. Chem.* **27**, 1787 (2006).
- [27] S. Grimme, S. Ehrlich, and L. Goerigk, *J. Comput. Chem.* **32**, 1456 (2011).
- [28] J. P. Perdew, K. Burke, and M. Ernzerhof, *Phys. Rev. Lett.* **77**, 3865 (1996).
- [29] A. A. Mostofi, J. R. Yates, G. Pizzi, Y.-S. Lee, I. Souza, D. Vanderbilt, and N. Marzari, *Comput. Phys. Commun.* **185**, 2309 (2014).
- [30] M. P. L. Sancho, J. M. L. Sancho, and J. Rubio, *J. Phys. F* **15**, 851 (1985).
- [31] Q.-S. Wu, S.-N. Zhang, H.-F. Song, M. Troyer, and A. A. Soluyanov, *Comput. Phys. Commun.* **224**, 405 (2018).
- [32] J. Gao, Q. Wu, C. Persson, and Z. Wang, [arXiv:2002.04032](https://arxiv.org/abs/2002.04032).
- [33] G. F. Koster, *Properties of the Thirty-Two Point Groups* (MIT Press, Cambridge, MA, 1963), Vol. 24.
- [34] A. A. Coelho, *J. Appl. Crystallogr.* **51**, 210 (2018).
- [35] G. Kresse and J. Hafner, *Phys. Rev. B* **49**, 14251 (1994).
- [36] G. Kresse and J. Furthmüller, *Phys. Rev. B* **54**, 11169 (1996).
- [37] G. Kresse and J. Furthmüller, *Comput. Mater. Sci.* **6**, 15 (1996).
- [38] P. E. Blöchl, *Phys. Rev. B* **50**, 17953 (1994).
- [39] G. Kresse and D. Joubert, *Phys. Rev. B* **59**, 1758 (1999).
- [40] R. Braithwaite, K. Mereiter, W. Paar, and A. Clark, *Mineral Mag.* **68**, 527 (2004).
- [41] D. E. Freedman, T. H. Han, A. Prodi, P. Müller, Q.-Z. Huang, Y.-S. Chen, S. M. Webb, Y. S. Lee, T. M. McQueen, and D. G. Nocera, *J. Am. Chem. Soc.* **132**, 16185 (2010).
- [42] T.-H. Han, J. S. Helton, S. Chu, D. G. Nocera, J. A. Rodriguez-Rivera, C. Broholm, and Y. S. Lee, *Nature (London)* **492**, 406 (2012).
- [43] Q. Wang, Q. Yin, and H. Lei, *Chin. Phys. B* **29**, 017101 (2020).
- [44] A. K. Nayak, J. E. Fischer, Y. Sun, B. Yan, J. Karel, A. C. Komarek, C. Shekhar, N. Kumar, W. Schnelle, J. Kübler *et al.*, *Sci. Adv.* **2**, e1501870 (2016).
- [45] N. Kiyohara, T. Tomita, and S. Nakatsuji, *Phys. Rev. Applied* **5**, 064009 (2016).
- [46] P. Vaqueiro and G. G. Sobany, *Solid State Sci.* **11**, 513 (2009).
- [47] Q. Xu, E. Liu, W. Shi, L. Muechler, J. Gayles, C. Felser, and Y. Sun, *Phys. Rev. B* **97**, 235416 (2018).
- [48] L. Fu and C. L. Kane, *Phys. Rev. B* **76**, 045302 (2007).
- [49] B. Singh, X. Zhou, H. Lin, and A. Bansil, *Phys. Rev. B* **97**, 075125 (2018).
- [50] I. Cucchi, A. Marrazzo, E. Cappelli, S. Riccò, F. Y. Bruno, S. Lisi, M. Hoesch, T. K. Kim, C. Cacho, C. Besnard, E. Giannini, N. Marzari, M. Gibertini, F. Baumberger, and A. Tamai, *Phys. Rev. Lett.* **124**, 106402 (2020).
- [51] R. Yu, H. Weng, Z. Fang, X. Dai, and X. Hu, *Phys. Rev. Lett.* **115**, 036807 (2015).
- [52] L. M. Schoop, L. S. Xie, R. Chen, Q. D. Gibson, S. H. Lapidus, I. Kimchi, M. Hirschberger, N. Haldolaarachchige, M. N. Ali, C. A. Belvin *et al.*, *Phys. Rev. B* **91**, 214517 (2015).
- [53] J. Nayak, S.-C. Wu, N. Kumar, C. Shekhar, S. Singh, J. Fink, E. E. Rienks, G. H. Fecher, S. S. Parkin, B. Yan *et al.*, *Nat. Commun.* **8**, 13942 (2017).
- [54] U. Rauchschwalbe, W. Lieke, F. Steglich, C. Godart, L. C. Gupta, and R. D. Parks, *Phys. Rev. B* **30**, 444 (1984).
- [55] H.-Y. Lu, N.-N. Wang, L. Geng, S. Chen, Y. Yang, W.-J. Lu, W.-S. Wang, and J. Sun, *Europhys. Lett.* **110**, 17003 (2015).
- [56] Z. Wang, P. Zhang, G. Xu, L. K. Zeng, H. Miao, X. Xu, T. Qian, H. Weng, P. Richard, A. V. Fedorov *et al.*, *Phys. Rev. B* **92**, 115119 (2015).
- [57] G. Xu, B. Lian, P. Tang, X.-L. Qi, and S.-C. Zhang, *Phys. Rev. Lett.* **117**, 047001 (2016).
- [58] X. Wu, S. Qin, Y. Liang, H. Fan, and J. Hu, *Phys. Rev. B* **93**, 115129 (2016).
- [59] P. Zhang, K. Yaji, T. Hashimoto, Y. Ota, T. Kondo, K. Okazaki, Z. Wang, J. Wen, G. Gu, H. Ding *et al.*, *Science* **360**, 182 (2018).
- [60] T. Machida, Y. Sun, S. Pyon, S. Takeda, Y. Kohsaka, T. Hanaguri, T. Sasagawa, and T. Tamegai, *Nat. Mater.* **18** 811, (2019).
- [61] L. Fu and E. Berg, *Phys. Rev. Lett.* **105**, 097001 (2010).
- [62] M. Kriener, K. Segawa, Z. Ren, S. Sasaki, and Y. Ando, *Phys. Rev. Lett.* **106**, 127004 (2011).
- [63] S. Sasaki, M. Kriener, K. Segawa, K. Yada, Y. Tanaka, M. Sato, and Y. Ando, *Phys. Rev. Lett.* **107**, 217001 (2011).
- [64] Z. Liu, X. Yao, J. Shao, M. Zuo, L. Pi, S. Tan, and C. Zhang, and Y. Zhang, *J. Am. Chem. Soc.* **137**, 10512 (2015).
- [65] G. Du, Y. Li, J. Schneeloch, R. Zhong, G. Gu, H. Yang, H. Lin, and H.-H. Wen, *Sci. China Phys. Mech.* **60**, 037411 (2017).
- [66] T. Sato, Y. Tanaka, K. Nakayama, S. Souma, T. Takahashi, S. Sasaki, Z. Ren, A. A. Taskin, K. Segawa, and Y. Ando, *Phys. Rev. Lett.* **110**, 206804 (2013).
- [67] M. Novak, S. Sasaki, M. Kriener, K. Segawa, and Y. Ando, *Phys. Rev. B* **88**, 140502(R) (2013).
- [68] C. M. Polley, V. Jovic, T.-Y. Su, M. Saghiri, D. Newby, Jr., B. J. Kowalski, R. Jakiela, A. Barcz, M. Guziewicz, T. Balasubramanian *et al.*, *Phys. Rev. B* **93**, 075132 (2016).